journal

J. Am. Ceram. Soc., 77 [7] 1719-28 (1994)

Nucleation and Growth of β′-SiAlON

Shyh-Lung Hwang† and I-Wei Chen*

Department of Materials Science and Engineering, University of Michigan, Ann Arbor, Michigan 48109-2136

Elongated β′-SiAlON grains grown from several fine-grained $Y_{m/3}Si_{12-(m+n)}Al_{m+n}O_nN_{16-n}$ compositions with α-Si_3N_4, AlN, Al_2O_3, and Y_2O_3 starting materials have been examined. These grains have large aspect ratios and are oriented along the [0001] axis. TEM structural and chemical analysis suggests that they are nucleated from various seed crystals, which can be α-Si_3N_4, β-Si_3N_4, or other β′-SiAlON. The β′-SiAlON seed and the initial precipitation on β-Si_3N_4 show a higher content of Al and O, indicating that a large transient supersaturation of Al and O in the liquid is instrumental for β′-SiAlON formation, whereas subsequent growth proceeds under a much lower driving force. The misfit between phases is accommodated by interfacial dislocations (*c*-type and *a*-type). Fully grown β′-SiAlON grains usually contain several variants independently nucleated from the same seed. In particular, the two alternative α/β phase-matching possibilities result in two [0001] growth habits separated by a twin boundary.

I. Introduction

The high fracture toughness found in some silicon nitride ceramics is associated with their unique microstructure containing an interlocking network of elongated β-Si_3N_4 or β′-SiAlON.[1] The development of such a microstructure goes through a solution/precipitation stage, in the presence of a liquid, into which the starting nitride powders are first dissolved before the final phase assemblage is formed. Starting powders with a high α-Si_3N_4 content have often been found to promote the formation of elongated β-Si_3N_4 or β′-SiAlON grains.[2-5] Lange[2] interpreted these results as indicating that β-Si_3N_4 particles in the starting powders served as nucleation sites for the elongated grains onto which the dissolved α-Si_3N_4 reprecipitated as β-Si_3N_4. While this view has been widely circulated, microscopy evidence for β-Si_3N_4 nucleation sites has not been detailed. This is partly because of the lack of a crystallographic or compositional "signature" of the seed β-Si_3N_4 grains which distinguishes them from the grown β-Si_3N_4 grains. In addition, since most researchers used a relatively high processing temperature for densifying Si_3N_4, the remnant nuclei may have disappeared in the process of homogenization and coarsening.

In a recent study of hot-pressing kinetics of SiAlON performed at relatively low temperatures using Si_3N_4, AlN, Al_2O_3, and Y_2O_3 as starting powders, we found the transient liquid initially rich in AlN, which apparently triggered the first precipitation in the form of supersaturated β′-SiAlON.[6] Subsequent precipitation continued on these early precipitates, but nucleation and growth of new precipitates onto other seeds, such as α-Si_3N_4 and β-Si_3N_4 also detected.[7] In all cases our observations were aided by the compositional, and in the case of α/β combination, the crystallographic, difference between the seed and the grown β′-SiAlON grains. The electron microscopy study of these phenomena, along with growth defects such as interfacial dislocations, twin boundary and twist boundary, is reported here. The implications of these observations on the microstructural development of β-Si_3N_4 and β′-SiAlON are also discussed. A parallel study of the nucleation and growth of α′-SiAlON is described elsewhere.[8]

II. Experimental Procedure

The main material reported here has a nominal composition $Y_{0.2}Si_{10.4}Al_{1.6}O_1N_{15}$ and was prepared by hot-pressing at 1550°C for 0.5 h. The starting powders are a Si_3N_4 (mostly α phase of medium size of 0.48 μm), AlN, Al_2O_3, and Y_2O_3. The details of the powder processing and hot-pressing procedures were given elsewhere for this composition and other SiAlONs.[6] The present composition, which falls on the so-called α′-plane with a general formula $Y_{m/3}Si_{12-(m+n)}Al_{m+n}O_nN_{16-n}$, contains nearly equal fractions of α′ and β′-SiAlON in its equilibrium phase assemblage.[9-11] It was referred to in Ref. 6 as material 0610 corresponding to $m = 0.6$ and $n = 1.0$. Since the as-hot pressed material contains a large amount of unreacted α-Si_3N_4, it was given a further annealing treatment at 1600°C for 1 h to somewhat coarsen the microstructure. The annealed material was then examined using a JEOL 2000 FX transmission electron microscope (TEM) which was operated at 200 kV and equipped with a thin-window EDS system. For the above study, the standard procedure for preparing thin foils was followed.[8] Additional discussion on the experimental methods regarding imaging conditions, EDS analysis, and the advantage of sampling statistics by using fine-grained materials can also be found in Ref. 8. Phase analysis was performed using X-ray diffraction (XRD) which determined the lattice parameters of α-Si_3N_4, α′-SiAlON, and β′-SiAlON. Scanning electron microscopy (SEM) was also employed for preliminary examination of the microstructure. Besides material 0610, several other SiAlON materials reported in Ref. 6 have been examined. They cover a broad range of phase assemblages, but all contain some amounts of β′-SiAlON. Despite the compositional difference, the main findings reported below were found generally applicable.

III. Results

(1) General Microstructure

In the as-hot-pressed state, the phase assemblage contains 27% α′-SiAlON, 9% β′-SiAlON, and 64% unreacted α-Si_3N_4. The material is fully dense and the microstructure contains mostly equiaxed α-Si_3N_4 and α′-SiAlON grains. The large equiaxed grains tend to be α′-SiAlON, and the smaller grains are unreacted α-Si_3N_4. This is quite similar to those reported by us for an assortment of superplastic SiAlONs.[12-14] Indeed, this material is superplastic, as verified by punch-stretching to large biaxial strains at 1550°C.[15]

After annealing, the phase assemblage becomes 50% α′-SiAlON and 50% β′-SiAlON with some unreacted α-Si_3N_4. The overall composition of β′-SiAlON was found to be close to β_{10}-SiAlON, i.e., $x = 0.8$ in the formula $Si_{6-x}Al_xO_xN_{8-x}$.[16]

T. E. Mitchell—contributing editor

Manuscript No. 194673. Received April 16, 1993; approved February 11, 1994.
Supported by the National Science Foundation under Grant No. DDM 9024975.
*Member, American Ceramic Society.
†Now at Oak Ridge National Laboratory, Metals and Ceramics Division, Oak Ridge, TN.

Thus, a larger extent of α-Si_3N_4 to β'-SiAlON transformation has taken place during annealing. The microstructure now contains elongated β'-SiAlON, as shown in Fig. 1, in addition to α'-SiAlON. The α'-SiAlON is usually found to surround an α-Si_3N_4 core (Fig. 1). Such growth morphology is characteristic of α'-SiAlON materials as described elsewhere for a $Y_{0.33}Si_{10}Al_2O_1N_{15}$ composition (m = 1.0 and n = 1.0) and was thought to indicate heterogeneous nucleation and epitaxial growth of α'-SiAlON on α-Si_3N_4.[8] Apparently this mechanism also operates in a composition less rich in α'-SiAlON. The most interesting new feature in Fig. 1, however, is the strong contrast, marked by arrows, in the central parts of the elongated grains. When the specimen is tilted, under the dark-field (DF) imaging conditions, the bright contrast always shifts from one end of the elongated grain to the other, as illustrated in Figs. 2(a–d). This means that there is some misorientation between the two ends of the elongated grain. A detailed analysis, described below, found that the strong contrast regions in the centers of these grains are either α-Si_3N_4, β-Si_3N_4, or supersaturated β'-SiAlON (richer in Al and O), while the bulk of the elongated grains is a β'-SiAlON of a lower Al and O composition (β_{10}-SiAlON). These cases are analyzed individually below.

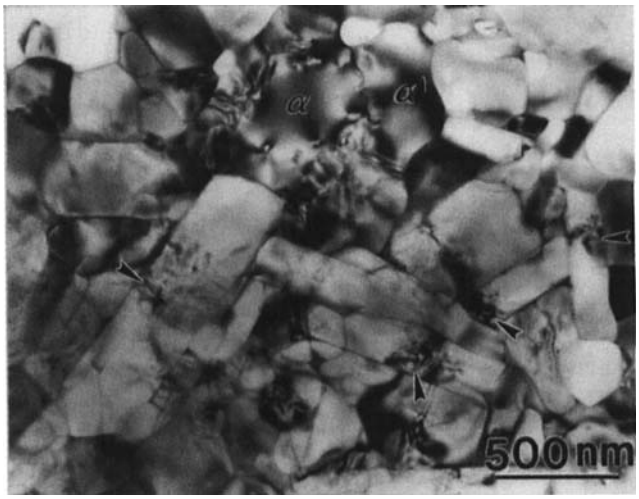

Fig. 1. BF image showing elongated β'-grains and an equiaxed α'-grain with a core/shell structure. The strain contrast in the center of β'-grains is marked by arrows.

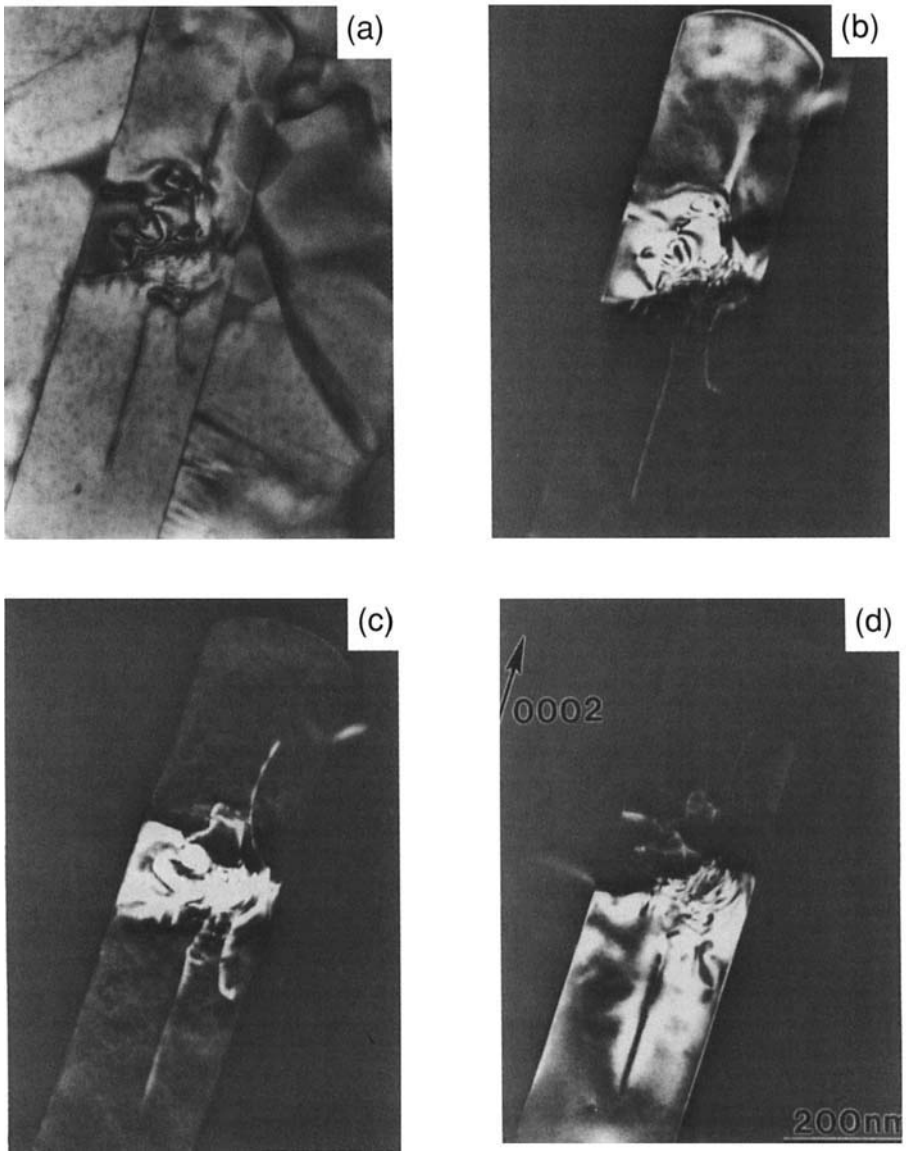

Fig. 2. (a) BF image of an elongated β' grain and (b–d) DF images showing that the contrast of the seed (center left) and of the upper and lower halves is shifted by tilting.

(2) Seeded Grain Structure

(A) α-Si_3N_4 Seed: Figure 3(a) is a TEM micrograph of an elongated β′-SiAlON grain containing a core and some type of planar defects. The planar defects, marked by an arrow head, are twin boundaries resulting from two different stacking sequences of β′-SiAlON, as will be analyzed in Section III(4)(A). The $10\bar{1}0$ reflection condition, Fig. 3(b), reveals the core to have a round morphology and a size of about 50 nm with Moiré fringes lining up parallel to the diffraction vector. This implies a small rotational misfit between the core and the shell. Selected area diffraction (SAD) patterns from the region that contains both the core and the outer grain (Fig. 4(a)) contain spots that belong to both an α and β-Si_3N_4 structure. Some spot splitting can be seen, indicating a small misorientation. However, if the core is excluded, then only diffraction spots of β-Si_3N_4 were obtained and the spot splitting disappeared (Fig. 4(b)). Thus, the core has an α-Si_3N_4 structure and the outer grains a β-Si_3N_4 structure, the two having nearly the same crystallographic orientation but for a small rotational misfit.

To perform energy-dispersive X-ray analysis (EDS), we have chosen the grain shown in Fig. 6 which has a core of α-Si_3N_4 structure not fully enclosed by the shell. The spectrum taken from this core (Fig. 5(a)) contains Si and N, with very weak peaks of Al and O. (The detection limit for Al and O is about 1.5 wt% in our instrument.) In contrast, the spectrum taken from the surrounding region (Fig. 5(b)) contains very strong peaks of Al and O in addition to Si and N. The above observation strongly suggests that the core is α-Si_3N_4, while the shell is β′-SiAlON. The very weak signal contributions of Al and O in Fig. 5(a) must come from the contamination of the surrounding β′-SiAlON and do not imply the core to be α′-SiAlON. This is because α′-SiAlON is expected to have a much higher Al and O content in the present system. Also, there is no Y in the core according to EDS, which would be expected if it were α′-SiAlON. The size of these α-Si_3N_4 cores is typically around 0.2 μm, somewhat smaller than the medium size of the starting powder. This may be attributed to partial dissolution during processing.

Figure 6(a) shows the elongated β′-SiAlON grain with an α-Si_3N_4 core on which the above EDS was performed. A higher-magnification weak-beam (WB) image of the core region is shown in Fig. 6(b). The microstructure in the center region was analyzed by SAD and EDS. It contains at least one α-Si_3N_4 region and a rounded β′-SiAlON region. According to the EDS analysis, this rounded β′-SiAlON is much richer in Al and O than the outer elongated β′ grain region; i.e., it is supersaturated.

Sometimes β′-SiAlON and α′-SiAlON grow simultaneously next to the same α-Si_3N_4 particle (Fig. 7). The growth direction

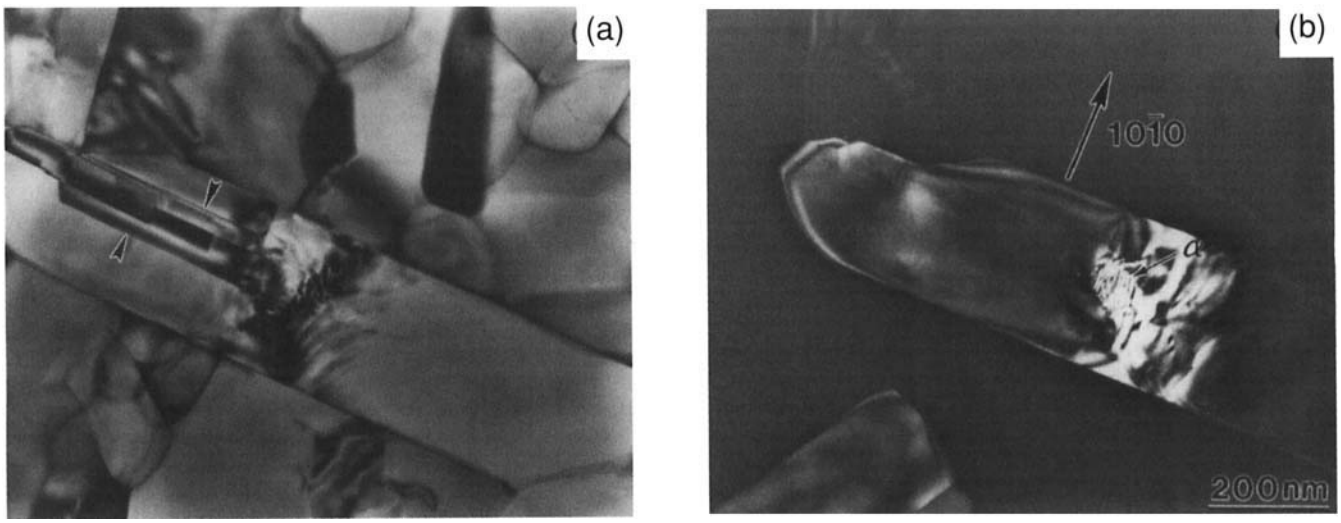

Fig. 3. (a) BF image and (b) DF image of a β′ grain with an α-Si_3N_4 seed. The twin boundaries are marked by an arrow in (a).

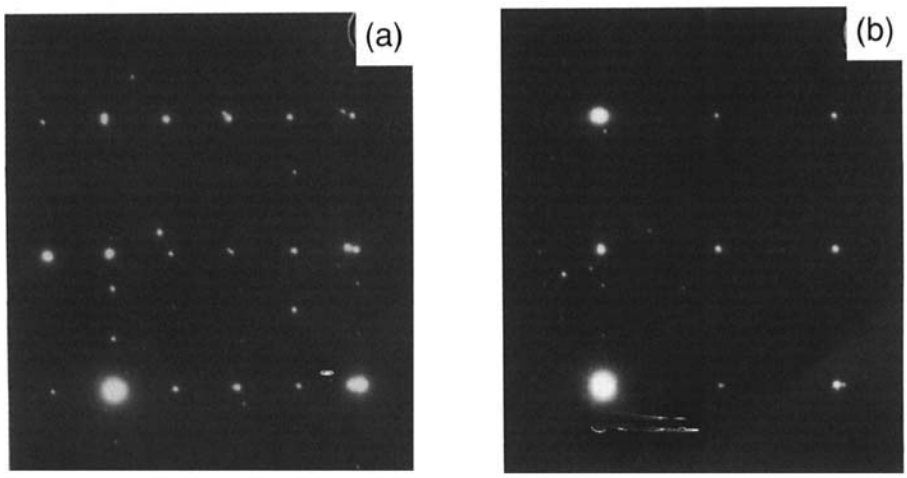

Fig. 4. SAD patterns of (a) β′-SiAlON shell + α-Si_3N_4 seed and (b) β′-SiAlON outer region alone. The extra spots in (a) indicate that the seed has an α-Si_3N_4 structure. B = $[41\bar{5}0]$.

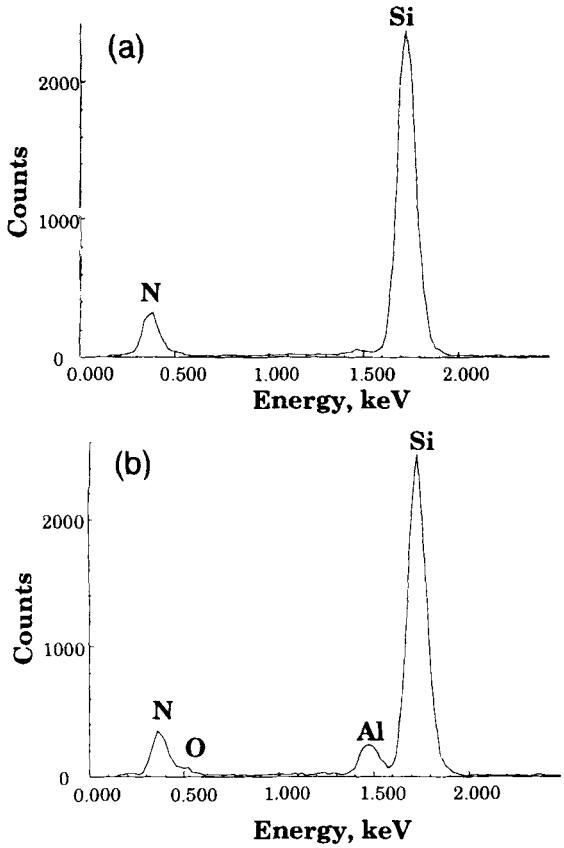

Fig. 5. EDS spectra of (a) α-Si_3N_4 seed and (b) β'-SiAlON outer region. The seed contains no Al or O.

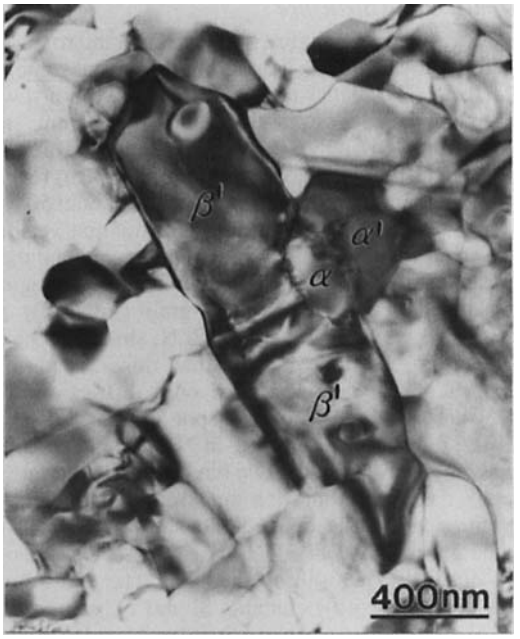

Fig. 7. BF image showing concurrent growth of β'-SiAlON and α'-SiAlON on an α-Si_3N_4 seed.

of the elongated β'-grain is along the *c*-axis, but all the phase regions have nearly the same crystallographic orientation with only a small misorientation. (α-Si_3N_4 and α'-SiAlON were distinguished by EDS.)

(B) β-Si_3N_4 Seed: Figure 8(a) shows an elongated β'-SiAlON grain with a β-Si_3N_4 core, as viewed under $(20\bar{2}0)$ diffraction condition. SAD patterns show that both the core and the outer grain have a β-Si_3N_4 structure and are in the same crystallographic orientation. EDS taken from a similar core not fully enclosed by the shell establishes that the core region (Fig. 9(a)) contains very little Al and O and, therefore, is probably pure β-Si_3N_4, while the shell (Fig. 9(b)) contains strong signals of Al and O and is definitely β'-SiAlON. The same region of Fig. 8(a) viewed under the (0002) reflection condition shows strong Moiré fringes with a spacing of about 7.1 nm. Thus, the lattice parameters along the *c*-axis have a misfit of 0.030 Å between the two phases, also indicating an *x* value of about 1.2 for the β'-SiAlON.[16]

The above configuration suggests that the β-Si_3N_4 is the seed for the β'-SiAlON grain. Note that the size of the β-Si_3N_4 core is quite small, around 50 nm, compared to the size of the starting powders. It typically has a rectangular shape with an aspect ratio of about 1.5 and is always embedded entirely in a β'-SiAlON shell.

(C) β'-SiAlON Seed: The grain shown in Figs. 2(a–d) is a β'-SiAlON with a supersaturated β'-SiAlON core. The core can be seen on the left center, along with dislocations threading

Fig. 6. (a) WB image of an elongated β'-SiAlON grain with twin boundaries and (b) complicated center region containing α-Si_3N_4 and a rounded supersaturated β'-SiAlON region.

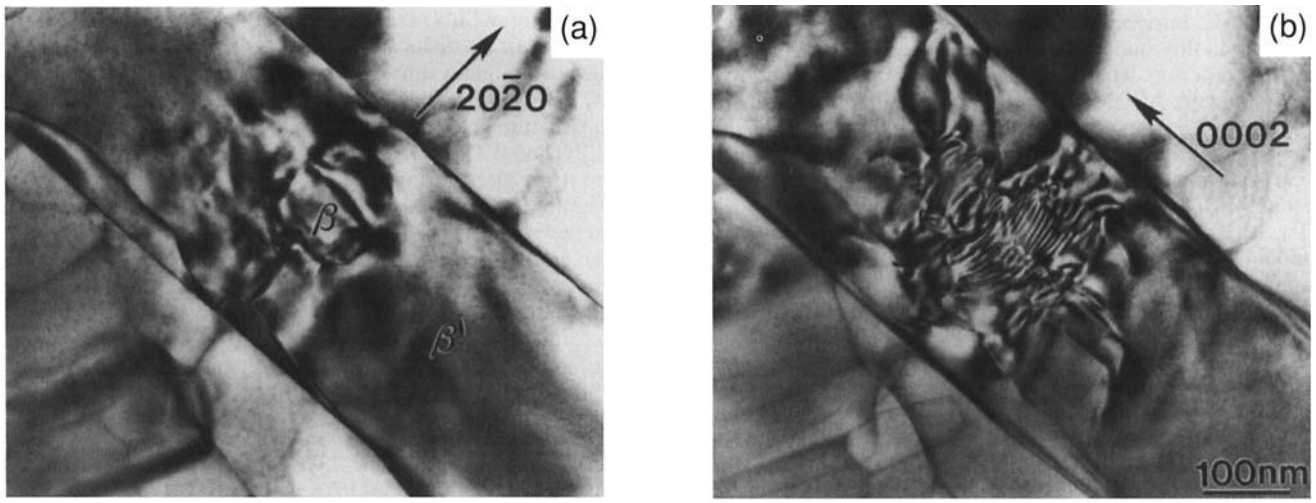

Fig. 8. BF images under (a) $20\bar{2}0$ and (b) 0002 reflections showing a β′-SiAlON grain with a β-Si_3N_4 seed. Moiré fringes are shown in (b).

from the interfaces in the upper and lower halves of the β′-SiAlON grain. SAD patterns from the core and the shell regions confirm that both have the same crystallographic orientation and a β-Si_3N_4 structure. The EDS spectra for this core (which is not fully embedded in the shell), as shown in Fig. 10(a), found Al and O with concentrations much higher than those in the outer region. We have estimated the core compositions to be in the range of $x \approx 2$ or β_{30}-SiAlON compared to the outer region of $x \approx 0.8$ or β_{10}-SiAlON. (For all the EDS spectra reported here, the spot size used was 10 nm, and the calibration for Si/Al ratio was performed by taking 10 measurements of a β'_{10}-SiAlON composition that gives the Cliff-Lorimer factor $K_{AlSi} = 1.19$.) Thus, the initial precipitation of β′-SiAlON that acts as the seed is much richer in Al and O than the later growth.

We have examined a large number of elongated β-SiAlON grains and always observed a strong contrast region in the center of these grains, suggesting the presence of the seeds. Similar observations of seeding configurations were also made for the 0625 material. The main difference in this material is a lower population of α′ grains as compared to the 0610 material, because of the higher Al content. The supersaturated β′-SiAlON core was found to have a composition close to β_{40} ($x = 3$), which is somewhat higher than that of the β′-SiAlON core in the 0610 material.

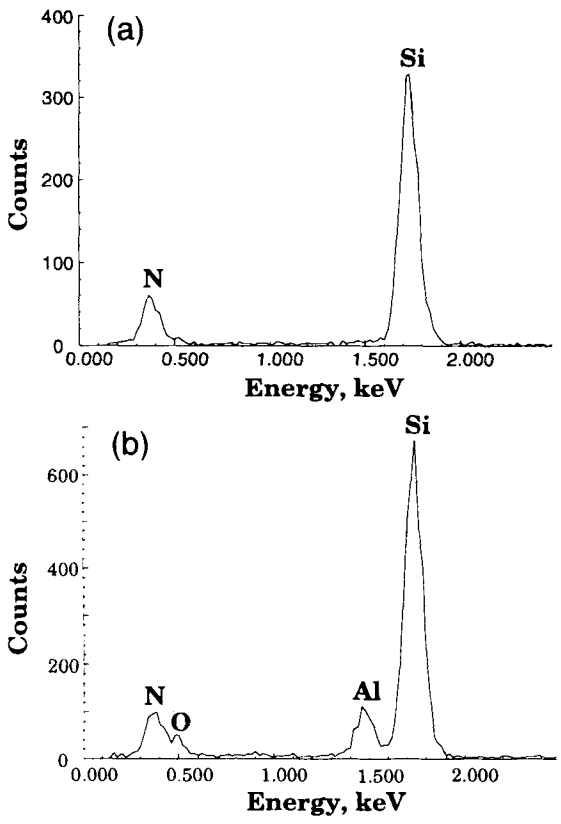

Fig. 9. EDS spectra of (a) β-Si_3N_4 seed and (b) β-SiAlON outer region. The seed contains Si and N only.

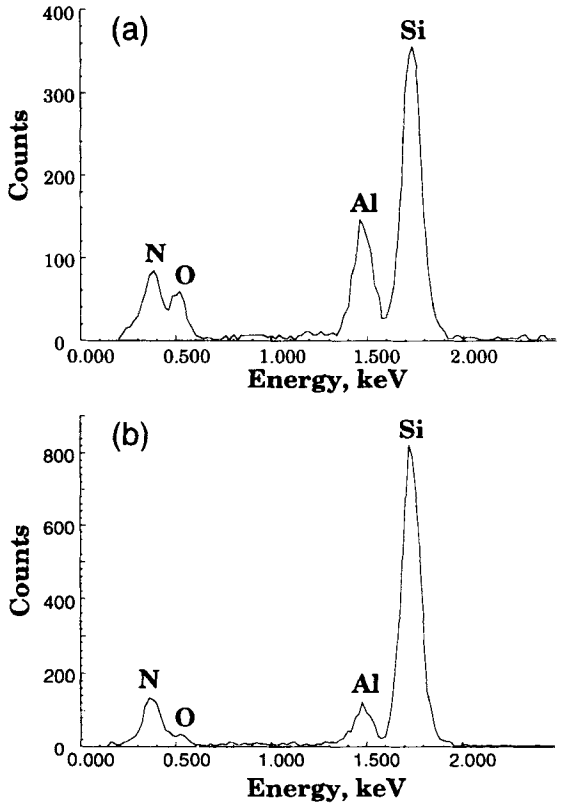

Fig. 10. EDS spectra of (a) supersaturated β′-SiAlON seed and (b) β′-SiAlON outer region. The Al and O contents are much higher in the seed than in the outer region.

(3) Interface Dislocations

(A) β/β′ *Interfaces:* Dislocations have been observed frequently in this study. They were analyzed using the conventional **g**·**b** criterion, where **g** is the operating reflection and **b** the Burgers vector. At least two nonparallel reflections that rendered the dislocation out of contrast were used to establish the dislocation character. To eliminate the interference from the Moiré fringes and to minimize the uncertainties of dislocation contrast, WBDF imaging was employed.

Two WB images of a typical misfit dislocation structure surrounding a β-Si_3N_4 seed are given in Fig. 11(a–b). These dislocations have a Burgers vector lying along the *c*-axis and are *usually* confined to a narrow region around the β-Si_3N_4 cores. The average spacing of these misfit dislocations, measured on several β/β′ interfaces, is around 125 Å. Assuming a Burgers vector of 2.91 Å, this corresponds to a lattice parameter misfit of 0.068 Å between the β and β′ phases along the *c*-axis. From the compositional dependence of β′-SiAlON, we calculate an *x* value of about 2.7 for the β′-SiAlON.[16] Note that, for this composition, the calculated lattice misfit along the *a*-axis between β and β′ phases, 0.074 Å, requires a set of *a*-axis dislocations spaced about 78 nm apart. Since the dimensions of the β-Si_3N_4 core are smaller than the latter value, no *a*-axis dislocation is expected.

(B) α/β′ *and* β′/β′ *Interfaces:* The dislocation structures surrounding α-Si_3N_4 seeds are usually complicated. As shown in Fig. 12(a), the dislocations are extended all the way from the center of the grain into the outer β′-SiAlON region. Many of these dislocations have a [0001] Burgers vector. This dislocation structure could result from either the large misfit between α-Si_3N_4 and β′-SiAlON or from the thermal mismatch between these two phases during cooling.

Figure 12(b) shows a dislocation network at the interface between a supersaturated β′-SiAlON seed and a β′-SiAlON outer grain. Although no detailed contrast analysis has been performed on this network, it is certain that at least two sets of dislocations are involved. This type of dislocation network usually forms when there is a rotational misfit.[17] A similar dislocation network can also be seen around the supersaturated β′-SiAlON grain shown in Fig. 6(b).

(4) Impingement Boundaries

(A) Twin Boundaries: The nature of the stacking sequences of atomic planes in the α- and β-Si_3N_4 structures dictates that the epitaxial growth of β′-SiAlON on α-Si_3N_4 can take place by two growth habits. Impingement of the two growth variants then results in a twin boundary, shown in Figs. 3 and 6, and serves as a distinct signature of β′-SiAlON

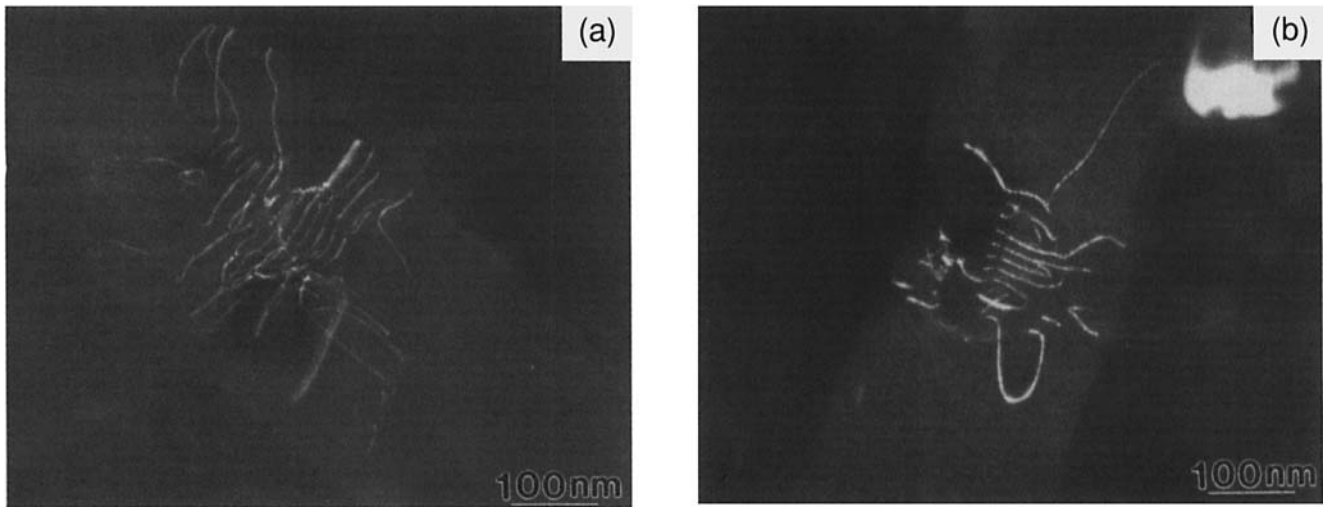

Fig. 11. WB images of interface dislocations around the β-Si_3N_4 seed. **g** = 0002.

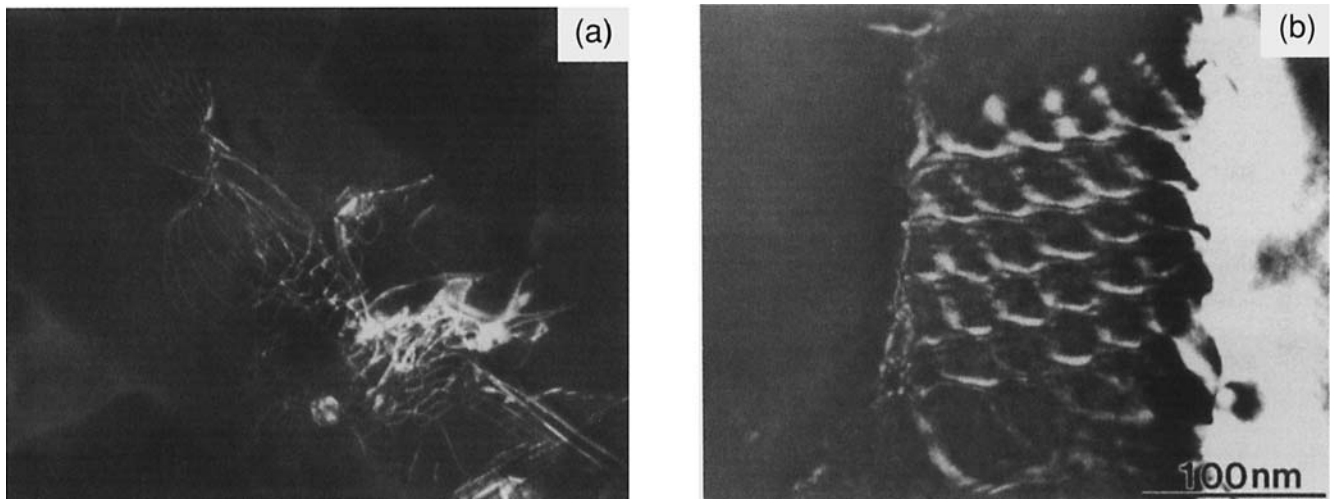

Fig. 12. WB images of (a) complicated dislocation structures in a β′-grain with an α-Si_3N_4 seed and (b) an interface dislocation network between a supersaturated β′-SiAlON seed and a β′-SiAlON outer region.

growth from an α-Si_3N_4 seed. The crystallographic origin of these twin planes and their identification are described below.

In α-Si_3N_4 structure, the C/D stacking layers are related to the A/B stacking layers by C-glide planes parallel to {1$\bar{1}$00}. Thus, when several β-Si_3N_4 nuclei grow epitaxially onto the surface of an α-Si_3N_4 crystal, they can adopt either the A/B stacking sequence or the C/D stacking sequence. Twin boundaries then form between the regions grown with A/B sequence and those with C/D sequence in the resulting β-Si_3N_4 grains. Assuming a (10$\bar{1}$0) boundary plane, the atomic configuration across such twin boundaries viewed along [0001] is shown in Fig. 13. The two parts of twins are related to each other by a reflection through the (10$\bar{1}$0) twin plane or by a 180° rotation about the [1$\bar{2}$10] direction. On the twin interface, each Si is coordinated by four N, and each N atom by three Si; i.e., all the Si–N bonds across the twin boundary are maintained. (There are some distortions of the bonding length and angle, though.) The presence of this kind of twin boundary originating from the α-Si_3N_4/β′-SiAlON interface in the as-grown elongated β′-SiAlON grains provides additional evidence for the seed nature of the α-Si_3N_4 core.

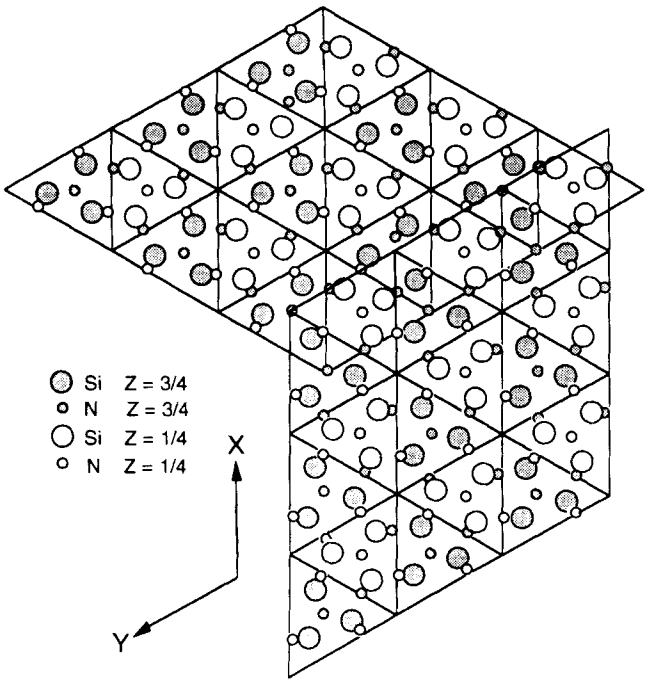

Fig. 13. Schematic atomic configuration of a (10$\bar{1}$0) twin viewed along [0001] with the twin boundary in edge-on position. Note continuity of Si–N bonding across the twin boundary.

A twin boundary can usually be ascertained by the appearance of twin spots in the SAD. Unfortunately, for {1$\bar{1}$00} twins in β′-Si_3N_4 crystals, no twin spots will appear in the SAD because {1$\bar{1}$00} are mirror planes of the reciprocal lattices. Therefore, the {1$\bar{1}$00} twins can be analyzed only by the structure factor contrast across the interface or by the diffraction contrast of the interface itself. The analysis is similar to the two-beam dynamical theory for the stacking fault contrast, because the crystal potential relationship between the two parts of the twinned crystal is similar to that in the stacking fault case.[17–20] The only difference is that the phase angle difference α_g of the gth Fourier coefficient of the lattice potential does not arise from a displacement, as in a stacking fault, but from a different structure across the interface, as in a twin boundary. The calculated structure factor values and the phase angle differences of a β-Si_3N_4 crystal twinned on the (10$\bar{1}$0) plane using this theory are listed in Table I. All reflections are indexed using β1 axes. Three groups of distinct structural factor contrast and predicted twin boundary visibility are exemplified in this table.

The above prediction has been verified by imaging under various DF conditions. For example, Fig. 14(a) shows a case, Group 1, for which there is no contrast difference across the boundary, which itself is visible. Likewise, Figs. 14(b) and (c) show two cases, Group 2, which have excited reflection from only one of the two twin variants and the boundary is again visible. Lastly, Fig. 14(d) shows a case, Group 3, which shows no contrast difference across the boundary, which itself is invisible.

(B) Twist Boundary: More than one growth variant is common for β′-SiAlON grown from a supersaturated β′-SiAlON seed. These variants typically have a small misorientation between them which can be revealed by systematic tilting, as evidenced in Figs. 2(a–d). When the two variants grow in the same direction from one side of the seed, their impingement results in a twist boundary. An example is shown in Figs. 15(a–d). In the BF image (Fig. 15(a)), the nature of twist misfit boundary is revealed by the Moiré fringes which are parallel to the operating reflection $\mathbf{g} = 01\bar{1}\bar{1}$. The contrast analysis of this boundary is given by the DF images in Figs. 15(b–d). Two sets of orthogonal interfacial dislocations can be observed in Fig. 15(b) for the reflection $\mathbf{g} = 0\bar{3}31$. One set of the dislocations is out of contrast when $\mathbf{g} = \bar{1}011$ and 0002, as in Fig. 15(c), while the other set is out of contrast when $\mathbf{g} = 0\bar{1}10$, $2\bar{3}10$, and $1\bar{4}30$, as in Fig. 15(d). These observations imply that one set of dislocations has a [0001] (c-axis) Burgers vector, while the other set has a 1/3 [1$\bar{2}$10] (a-axis). By comparing the BF micrograph with the SAD pattern, it is noted that all the interfacial dislocations have only a screw character, indicating that there is no, or only very limited, lattice parameter misfit between these two growth variants.[21] This observation is also confirmed by the EDS analysis, which detects no compositional difference.

Table I. Structure Factor, Phase Angle Difference, and Diffraction Contrast of Twin Boundary in β′-SiAlON*

Group	Reflections	Structure factor, β1	Structure factor, β2	Phase angle difference	Struct. fac. contrast	Boundary visibility
1	01$\bar{1}$1	12.97	12.97	2/3π	No	Visible
	10$\bar{1}$1	12.97	12.97	2/3π	No	Visible
	$\bar{1}$011	12.97	12.97	2/3π	No	Visible
	20$\bar{2}$1	7.09	7.09	4/3π	No	Visible
2	$\bar{2}\bar{3}$51	13.32	4.34	2/3π	Yes	Visible
	21$\bar{3}$0	17.37	0.58	4/3π	Yes	Visible
	3$\bar{2}$10	17.37	0.58	2/3π	Yes	Visible
	31$\bar{2}$0	0.58	17.37	4/3π	Yes	Visible
3	0002	20.56	20.56	0	No	Invisible
	1$\bar{1}$20	7.89	7.89	0	No	Invisible
	$\bar{1}$121	4.89	4.89	0	No	Invisible

*The twin plane is (10$\bar{1}$0), which passes through (1/3, 2/3, 0) point. All reflections were indexed using β1 axes. The structure factors were calculated assuming 100% occupancy of the atomic positions by Si or N. The substitution of Al for Si and O for N in β_{10}-SiAlON will result in small changes in the structure factors, but the ratios for the structure factors and the phase angle differences between β1 and β2 should remain the same.

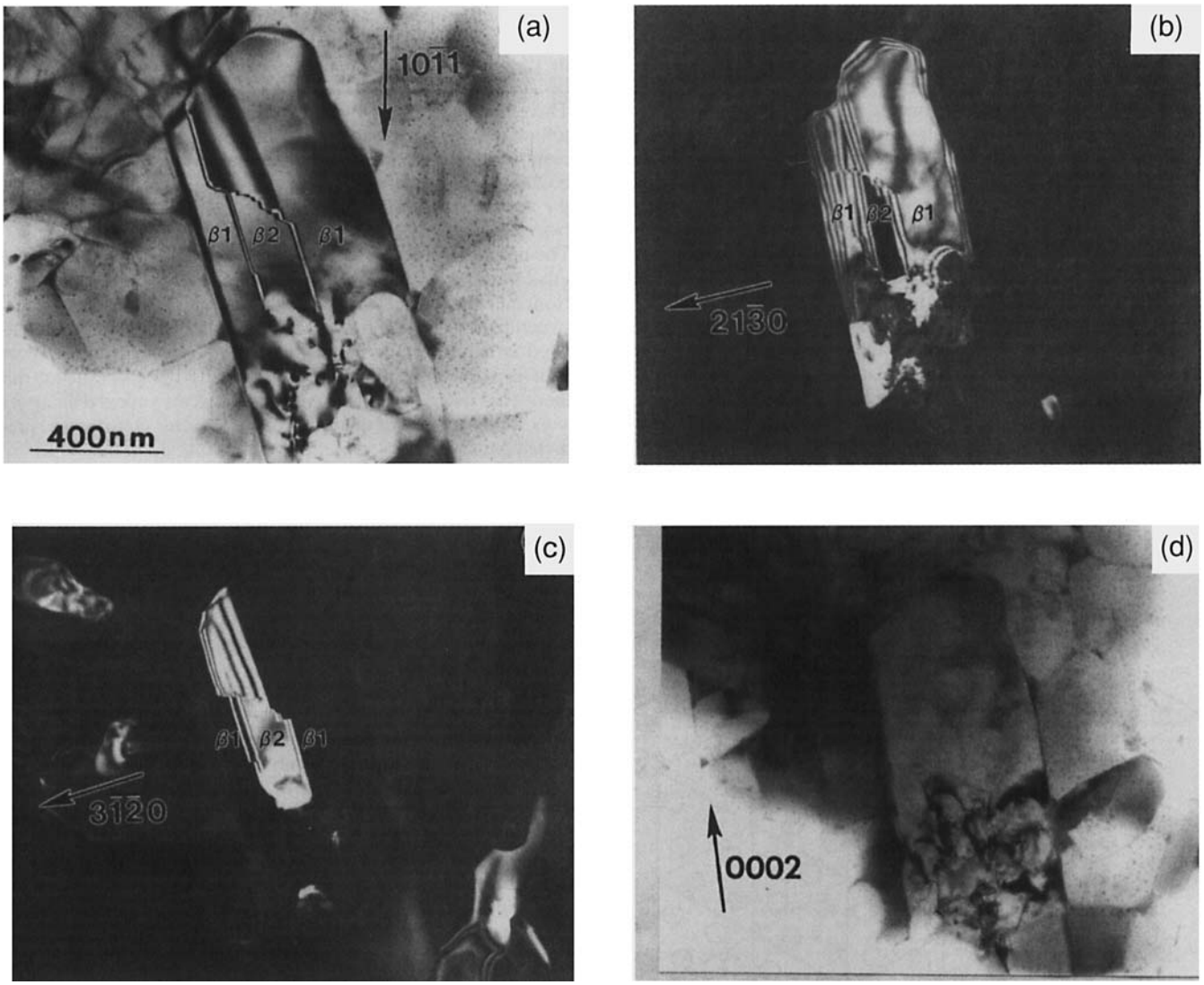

Fig. 14. TEM two-beam images of $(10\bar{1}0)$ twins. (a) Twin boundaries visible and no structure factor contrast between β1 and β2, $\mathbf{g} = 10\bar{1}1$; (b) β1 with a large structure factor and β2 with a small structure factor, $\mathbf{g} = 21\bar{3}0$; (c) opposite to (b), $\mathbf{g} = 3\bar{1}\bar{2}0$; and (d) twin boundary invisible and no structure factor contrast between β1 and β2, $\mathbf{g} = 0002$.

The twist angle θ between these two variants can be calculated from the Burgers vector and the dislocation spacing s using $\theta = b/s$. The Burgers vectors are 7.61 and 2.91 Å, respectively, for the a-axis and the c-axis dislocations, and the corresponding spacings are 215 and 82 Å, respectively. The calculated twist angle is then 2.05° from both sets of data. This value is confirmed by another calculation from the Moiré fringe spacing, s_m, using[21] $s_m = d^2/(2d^2(1 - \cos(\theta)))$ where d is the corresponding d-spacing of the operating reflection. The fringe spacing is 66.7 Å in Fig. 15(a) under the $(01\bar{1}\bar{1})$ reflection. Therefore, the twist angle is 2.20°.

IV. Discussion

(1) Microstructural Development

(A) Heterogeneous Nucleation: The present TEM results indicate that epitaxial heterogeneous nucleation, which is the primary nucleation mechanism in the α-Si_3N_4 to α′-SiAlON phase transformation as discussed in a previous paper,[8] is also likely to be important in the α-Si_3N_4 to β′-SiAlON transformation in the α′ + β′-SiAlON materials at 1600°C. Evidence for nucleation sites has been found for both the preexisting α and β-Si_3N_4 grains from the starting powder and for the supersaturated β′-SiAlON grains. Similar observations of a supersaturated core for the β′-SiAlON grains have been obtained in composition $m = 0.6$, $n = 2.5$ (material 0625) and $m = 0.6$, $n = 5.0$ (material 0650) studied in Ref. 6. The intergrowth of β′-SiAlON and other crystals—α-Si_3N_4, β-Si_3N_4, and supersaturated β′-SiAlON—cannot be simply dismissed as growth impingement, because the latter are always found to be contained in the much larger and elongated β′-SiAlON grains. In addition, there are definite signatures of grains growing from different seed crystals; for example, twin boundaries are found only when the seed is α-Si_3N_4. Although we cannot entirely rule out the possibility of homogeneous nucleation, our experience of always finding a strong contrast region within the elongated β′-SiAlON grain strongly suggests that heterogeneous nucleation is likely and perhaps dominant.

The source of the supersaturated β′-SiAlON seeds which are so generally found in the present study is understandable.[6,7] During reaction of α-Si_3N_4, AlN, Al_2O_3, and Y_2O_3, a ternary Si-Al-Y oxide melt forms at 1350°C. Subsequently, AlN dissolves first, causing a large supersaturation of Al and N, triggering precipitation of β′-SiAlON of a high Al and O content. (This process may involve homogeneous nucleation or, as suggested by Fig. 6(b), heterogeneous nucleation on α-Si_3N_4.) The supersaturation is later relieved by dissolution of α-Si_3N_4. The secondary growth of β′-SiAlON is thus under a relatively small driving force and attains a composition representative of the overall one. In the present case of α′ + β′-SiAlON, the final

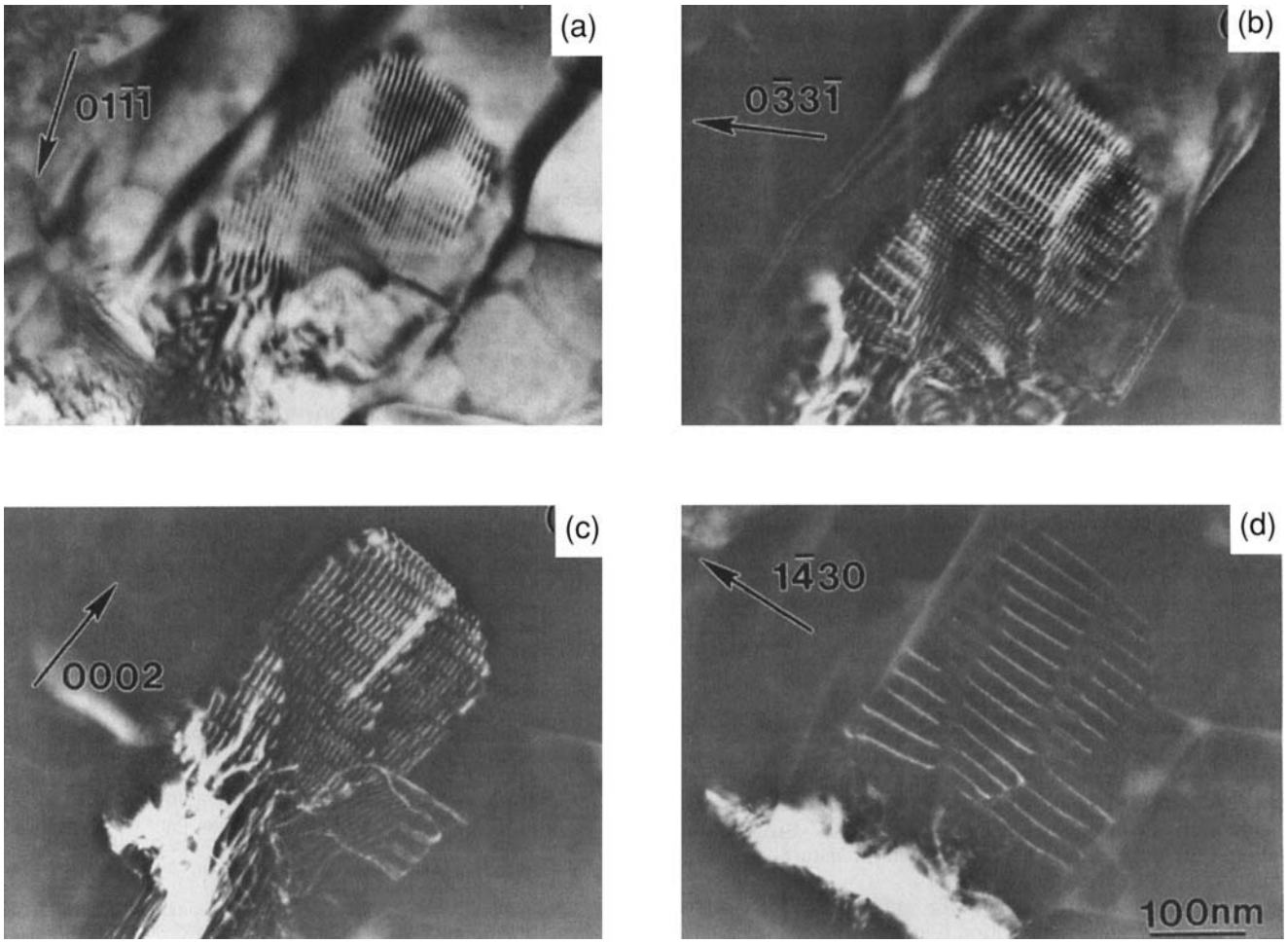

Fig. 15. (a) BF and (b–d) WB images of a twist boundary between two β′ variants.

β′-SiAlON should have the β_{10}-SiAlON composition according to the recently established subsolidus phase relationships.[10,11] This has been confirmed by XRD analysis of β′-SiAlON in the bulk.

The case of β-Si_3N_4 acting as a seed requires some elaboration. According to the dislocation analysis (Section III(3)(A)), the β′-SiAlON grown onto the seed has a composition of $x = 2.7$, i.e., β_{40}. Moiré fringe analysis (Section III(2)(B)), however, gives $x = 1.2$ or β_{20}. Meanwhile, the EDS analysis (Fig. 9(b)) gives $x = 0.8$ or β_{10}. These various results can be understood if we assume that the first layer grown onto the β-Si_3N_4 seed is highly supersaturated, with a composition similar to that determined by the interface dislocation spacing, while the subsequent growth involves progressively lower supersaturation ranging from that given by the Moiré fringe analysis to that given by the EDS analysis. This scenario is consistent with our interpretation that a high supersaturation initially exists in the liquid. Theoretically, the difference in the formation enthalpy between α-Si_3N_4 and β-Si_3N_4 is only about 30 kJ/mol,[22] or 1/25 of the formation enthalpy of either phase.[23] Thus, the driving force for α ⟶ β transformation is quite small unless an additional driving force from AlN supersaturation is present. This is the case in the early transient following AlN dissolution. Later, the large driving force is dissipated by β′-SiAlON precipitated by more α-Si_3N_4 dissolution.

The fact that α-Si_3N_4 particles do act as nuclei is particularly revealing. This is because the interfacial energy at the α/β interface is higher than that at the β/β interface, due to the difference in the stacking sequence in the two structures.[24] Also, the lattice misfit is relatively large (0.055 along the *c*-axis and −0.0095 along the *a*-axis between α-Si_3N_4 and β_{40}-SiAlON versus 0.022 and 0.0095 between β-Si_3N_4 and β_{40}-SiAlON).[10,16] This should render α-Si_3N_4 unfavorable for epitaxial nucleation unless (a) there is a severe difficulty for homogeneous nucleation, and (b) other more favorable nucleation sites, such as β-Si_3N_4 and supersaturated β′-SiAlON, have already been exhausted. This is quite reasonable in the present case, since the amount of preexisting β-Si_3N_4 in the starting powders is small, and supersaturated β′-SiAlON crystals form only over a brief transient.[6]

As mentioned in the Introduction, although the microstructural development in α ⟶ β transformation of silicon nitride has been very extensively studied in the past,[1–5,25–30] direct microscopic information on transformation nuclei is still very limited.[27] In this study, the often invoked proposal that the β-Si_3N_4 particles in the starting powder can act as nuclei for β-Si_3N_4 (or β′-SiAlON) has found some microscopic evidence. However, we also found that other nuclei, including α-Si_3N_4 and supersaturated β′-SiAlON, are operational. This lack of uniqueness of the nuclei must be borne in mind in reviewing microstructural development data of silicon nitride.

(B) Growth Anisotropy: In an experiment performed by Wotting *et al.*,[4] it was found that the resulting aspect ratio of the β-Si_3N_4 grains strongly depends on the eutectic temperature of the grain boundary liquid phase. They argued that supersaturation is required to produce elongated grain morphology through idiomorphic nucleation and crystallization. The more viscous (higher eutectic temperature) the grain boundary liquid phase is, the slower the supersaturation dissipates, and a higher aspect ratio of the β-Si_3N_4 grains results.

In the present experiment, the viscosity of the melt should be higher than that in the materials studied by Wotting *et al.*,

because of the higher nitrogen content. In contrast to their prediction, no elongated grains precipitated out directly from the melt. Instead, the initial supersaturation apparently facilitated the nucleation of the supersaturated β-SiAlON grains, which are mostly equiaxed. The subsequent growth of equilibrium β′-SiAlON on these seeds is much more anisotropic, despite a much lower supersaturation. These results lend no support to Wotting's picture.

An alternative interpretation of anisotropic growth of β-Si_3N_4 and β′-SiAlON has been recently put forth following the concept of roughening transition.[7] Experimentally, it is well-established that the slow growth direction, along the *a*-axis, has an atomically flat interface, while the fast growth direction, along the *c*-axis, has a rounded and atomically rough interface.[26] (The origin of these different interface structures can be rationalized in terms of bond continuity considerations.[15,31]) Kinetically, it follows that the rough interface should have a normal growth rate, while the flat interface growth is rate-limited by the lack of growth steps. This leads to a growth anisotropy which is particularly severe at low driving forces. On the other hand, at high driving forces, the flat interface receives enhanced step nucleation and becomes "kinetically" roughened.[32] As a result, growth anisotropy is lessened. These predictions are consistent with the results reported above.

V. Conclusions

(1) Microscopy evidence has been obtained which suggests β′-SiAlON grains nucleating from α-Si_3N_4, β-Si_3N_4, and other β′-SiAlON seed crystals.

(2) The initial precipitation and the β′-SiAlON seeds show a higher content in Al and O, indicating that a large supersaturation in Al and O in the liquid is instrumental for β′-SiAlON formation. The supersaturation is transient in nature, resulting from preferential dissolution of AlN.

(3) Regardless of the seed, the subsequent β′-SiAlON growth at equilibrium composition is anisotropic, along [0001], giving a highly elongated appearance for the grain, with its transverse dimension about two to three times that of the seed.

(4) Fully grown β′-SiAlON grains contain several variants independently nucleated from the same seed. In the case of α-Si_3N_4 seeding, a special twin boundary forms between variants, following the two matching alternatives at the α′/β interface.

(5) Interfacial dislocations (*c*-type and *a*-type) are commonly present in β′-SiAlON to accommodate lattice mismatch.

References

[1]E. Tani, S. Umebayashi, K. K. Kikobayashi, and M. Nishijima, "Gas Pressure Sintering of Si_3N_4 with Concurrent Additives of Al_2O_3 and 5 wt% Rare Earth Oxide: High Fracture Toughness Si_3N_4 with Fiber-Like Structure," *Am. Ceram. Soc. Bull.*, **65** [9] 1311–15 (1986).

[2]F. F. Lange, "Fracture Toughness of Si_3N_4 as a Function of the Initial α-Phase Content," *J. Am. Ceram. Soc.*, **62** [9–10] 428–30 (1979).

[3]G. Himsolt, H. Knoch, H. Huebner, and F. W. Kleinlein, "Mechanical Properties of Hot-Pressed Silicon Nitride with Different Glass Structures," *J. Am. Ceram. Soc.*, **62** [1–2] 29–32 (1979).

[4]G. Wotting, B. Kanka, and G. Ziegler, "Microstructural Development, Microstructural Characterization and Relation to Mechanical Properties of Dense Silicon Nitride"; pp. 83–96 in *Non-Oxide Technical and Engineering Ceramics*. Edited by S. Hampshire. Elsevier Applied Science, London, U.K., 1986.

[5]M. Mitomo, M. Tsutsumi, H. Tanaka, S. Uenosono, and F. Saito, "Grain Growth during Gas-Pressure Sintering of β-Silicon Nitride," *J. Am. Ceram. Soc.*, **73** [8] 244–45 (1990).

[6]S.-L. Hwang and I-W. Chen, "Reaction Hot-Pressing of Si_3N_4 and SiAlON Ceramics," *J. Am. Ceram. Soc.*, **77** [1] 165–71 (1994).

[7]I-W.Chen and S.-L. Hwang, "Superplastic SiAlON—A Bird Eye's View of Silicon Nitride Ceramics"; pp. 209–22 in *Silicon Nitride Ceramics—Scientific and Technological Advances*. Edited by I-W. Chen, P. F. Becher, M. Mitomo, G. Petzow, and T. S. Yen. MRS Symposium Proceedings, V. 287. Materials Research Society, Pittsburgh, PA, 1993.

[8]S.-L. Hwang and I-W. Chen, "Nucleation and Growth of α′-SiAlON," *J. Am. Ceram. Soc.*, in review.

[9]S. Slasor and D. P. Thompson, "Preparation and Characterization of Yttrium α′-SiAlONs"; see Ref. 4, pp. 223–30.

[10]W. Y. Sun, T.-Y. Tien, and T. S. Yen, "Solubility Limits of α′-SiAlON Solid Solutions in the System Si,Al,Y/N,O," *J. Am. Ceram. Soc.*, **74** [10] 2547–50 (1991).

[11]W. Y. Sun, T.-Y. Tien, and T. S. Yen, "Subsolidus Phase Relationships—Part of the System Si,Al,Y/N,O: The System Si_3N_4–AlN–YN–Al_2O_3–Y_2O_3," *J. Am. Ceram. Soc.*, **75** [11] 2753–58 (1992).

[12]I-W.Chen and L. A. Xue, "Development of Superplastic Structural Ceramics," *J. Am. Ceram. Soc.*, **73** [9] 2585–609 (1990).

[13]I-W. Chen and S.-L. Hwang, "Shear Thickening Creep in Superplastic SiAlONs," *J. Am. Ceram. Soc.*, **75** [5] 1073–79 (1992).

[14]X. Wu and I-W. Chen, "Exaggerated Textures and Grain Growth in a Superplastic SiAlON," *J. Am. Ceram. Soc.*, **75** [10] 2733–41 (1992).

[15]S.-L. Hwang, "Fabrication, Microstructural Characterization and Deformation of Superplastic Sialon Ceramics"; Ph.D. Dissertation. University of Michigan, Ann Arbor, MI, 1992.

[16]M. Havier and O. Johannesen, "Unit-Cell Dimension of β′-SiAlON," *Adv. Ceram. Mater.*, **3** [4] 405–407 (1988).

[17]M. J. Whelan, "Dynamic Theory of Electron Diffraction"; pp. 43–106 in *Diffraction and Imaging Techniques in Material Science*. Edited by S. Amelinckx, R. Gevers, and J. Van Landuyt. North-Holland, New York, 1978.

[18]S. Amelinckx and J. Van Landuyt, "The Study of Planar Interfaces by Means of Electron Microscopy"; see Ref. 17, pp.107–51.

[19]O. Biest and G. Thomas, "Identification of Enantiomorphism in Crystals by Electron Microscopy," *Acta Crystallogr.*, **A30**, 70–76 (1975).

[20]R. Gevers, "On the Dynamic Theory of Different Types of Electron Microscopic Transmission Fringe Patterns," *Phys. Status Solidi*, **3**, 1672 (1963).

[21]M. Hwang, D. E. Laughling, and I. M. Bernstein, "Interphase Interfaces of Au-Ag and Au-Pd," *Acta Metall.*, **28**, 621–32 (1980).

[22]R. Grun, "The Crystal Structure of β′Si_3N_4: Structural and Stability Consideration between α- and β-Si_3N_4," *Acta Crystallogr.*, **B35**, 800–804 (1979).

[23]R. D. Pehlke and J. F. Elliott, "High Temperature Thermodynamics of the Silicon, Nitrogen, and Silicon Nitride System," *Trans. Metall. Soc. AIME*, **21**, 781–85 (1956).

[24]D. P. Thompson, "The Crystal Chemistry of Nitrogen Ceramics," *Mater. Sci. Forum*, **47**, 21–24 (1989).

[25]D.-D. Lee, S.-J. L. Kang, and D. N. Yoon, "Mechanism of Grain Growth and α–β′ Transformation during Liquid-Phase Sintering of β′-SiAlON," *J. Am. Ceram. Soc.*, **71** [9] 803–806 (1988).

[26]C. M. Hwang, T.-Y. Tien and I-W. Chen, "Anisotropic Grain Growth during Final Stage Sintering of Silicon Nitride Ceramics"; pp. 1304–45 in *Sintering 87*. Edited by S. Somiya, M. Shimada, M. Yoshimura, and R. Watanabe. Elsevier Applied Science, New York, 1988.

[27]C. Chatfield, T. Ekström, and M. Mikus, "Microstructural Investigation of Alpha–Beta Yttrium SiAlON Materials," *J. Mater. Sci.*, **21**, 2297–307 (1986).

[28]D. R. Messier, F. L. Riley, and R. J. Brook, "The α/β Silicon Nitride Phase Transformation," *J. Mater. Sci.*, **13**, 1199–205 (1978).

[29]M. Fukuhara, "Effect of Nitrogen on the α/β Phase Conversion in Silicon Nitride," *J. Am. Ceram. Soc.*, **68** [9] C-226–C-228 (1985).

[30]J. Y. Park, J. R. Kim, and C. H. Kim, "Effect of Free Silicon on the α to β Phase Transformation in Silicon Nitride," *J. Am. Ceram. Soc.*, **70** [10] C-240–C-242 (1987).

[31]P. Hartman, "Structure and Morphology"; pp. 367–402 in *Crystal Growth: An Introduction*. Edited by P. Hartman. North-Holland, Amsterdam, Holland, 1973.

[32]G. H. Gilmer and K. A. Jackson, "Computer Simulation of Crystal Growth"; pp. 80–114 in *Crystal Growth and Materials*. Edited by E. Kaldis and H. J. Scheel. North-Holland, Amsterdam, Holland, 1977. □